# 3D Particle-in-Cell Modeling of $E \times B$ Discharge

# IEPC-2025-492

Presented at the 39th International Electric Propulsion Conference, Imperial College London, London,
United Kingdom
14-19 September 2025

Andrew C. Denig\* and Ken Hara<sup>†</sup>

Stanford University, Stanford, CA, 94305, U.S.A

Electron cyclotron drift instability (ECDI) and modified two-stream instability (MTSI) are two kinetic instabilities that occur within partially magnetized plasmas. The interaction of the plasma waves induced by these instabilities with the electrons is thought to enhance the transport of these electrons across magnetic field lines in Hall thrusters. A 3D particle-in-cell code is developed to study these phenomena and to verify the kinetic theory of these two instabilities. MTSI is found to be sensitive to the radial boundary condition. While MTSI does not appear with periodic radial boundary conditions, with grounded, radial walls, the plasma-wall interaction facilitated the growth of MTSI in accordance with linear perturbation theory. Furthermore, by varying the initial ion temperature, the growth rate of ECDI was affected in a way that was predicted by the kinetic theory. As the ion population became hotter, the growth rate of ECDI decreased due to ion Landau damping. This damping persists, even after the saturation of the instability, so for cases with  $T_{i,0} > 2$  eV, the plasma eventually returns to quiescence.

# I. Nomenclature

 $\mathbf{k}$  = wavevector

k = magnitude of wavevector

 $k_{\perp}$  = wavevector component perpendicular to applied magnetic field

 $k_{\parallel}$  = wavevector component parallel to applied magnetic field

 $\lambda_D$  = Debye length

 $\omega$  = complex wave frequency

 $\omega_r$  = real frequency

 $\gamma$  = growth rate

 $\mathbf{U}_{i}^{+} = \text{singly-chargedi on bulk velocity}$ 

 $r_L$  = Larmor radius

 $\mathbf{U}_d = E \times B \text{ drift velocity}$ 

 $\omega_{ce}$  = electron cyclotron frequency

<sup>\*</sup>PhD Candidate, Aeronautics and Astronautics, adenig3@stanford.edu
†Assistant Professor, Aeronautics and Astronautics, and kenhara@stanford.edu.



# II. Introduction

Hall thrusters<sup>1</sup> are devices that use perpendicular, applied electric and magnetized fields to confine electrons within the discharge channel via  $E \times B$  drift motion. A neutral gas, typically a noble gas due to their low ionization energies and large atomic masses, is injected through the anode plane. This neutral gas is ionized by the confined electrons to produce the ions desired for thrust. The device scale is smaller than the ion Larmor radius, so the ions are effectively unmagnetized, only feeling the effects of the axial electric field. Devices like this are said to contain partially magnetized plasmas. The confinement time of the electrons is directly related to the cathode efficiency of the Hall thruster. However, it has been experimentally demonstrated that the mobility of electrons across magnetic field lines is roughly an order of magnitude higher than what is expected from electron-neutral collisions alone.<sup>2-4</sup> It is hypothesized that this anomalous electron transport is driven by the plasma turbulence resulting from various plasma instabilities. The instabilities are electrostatic because the wavevector is parallel to the oscillating electric field, both of which are in the azimuthal  $(E \times B)$  direction within the Hall thruster channel. The two main electrostatic, kinetic instabilities of interest in partially magnetized plasmas are electron cyclotron drift instability (ECDI)<sup>5-7</sup> and modified two-stream instability (MTSI).<sup>8,9</sup> ECDI and MTSI are excited by free energy from the relative drift of the electrons with respect to the ions. ECDI is a short-wavelength (millimeter-scale) oscillation with a frequency of 1-10 MHz, while MTSI is a long-wavelength (centimeter scale) oscillation with a frequency of 0.1-1 MHz.

Because ECDI and MTSI are kinetic in nature, traditional fluid models are not capable of accurately capturing the small wavelength modes of these instabilities. Instead, kinetic models are required, namely using the particle-in-cell (PIC) approach. Previous one-dimensional (1D)<sup>10,11</sup> models have been used to model the  $E \times B$  direction, but these models are not able to capture self-consistent behavior along the magnetic field lines, and as such, cannot capture MTSI. Likewise, two-dimensional (2D) PIC models<sup>12–16</sup> can either capture self-consistent coupling of the particles and fields in the planes normal to the magnetic field or the electric field. However, in the first case, MTSI cannot appear, and in the second case, the anomalous mobility cannot be computed. Therefore, three-dimensional (3D) PIC models are necessary to capture the appearance of ECDI, MTSI, and their impact on the electron mobility. Taccogna<sup>17</sup> and Villafana<sup>18</sup> have previously developed 3D PIC simulations of Hall thruster geometries. However, Taccogna scaled the geometric scale by a factor of 10 while increasing the magnitude of the magnetic field and particle density by the same factor. Changing the magnetic field and particle density alters the growth rate, frequency, and wavelength of ECDI and MTSI. Furthermore, both Taccogna and Villafana included additional effects like electron-neutral collisions or a prescribed ionization profile, secondary electron emission, and/or a realistic magnetic field profile. As a result, it is difficult to decouple these effects from each other to study the 3D effects of MTSI and ECDI directly.

Here, a 3D test case is sought that highlights the additional effects that ECDI and MTSI have when modeled in 3D compared to 1D or 2D. The PIC results are compared to theoretical predictions from the ECDI and MTSI dispersion relations. The code structure will be briefly described before elucidating the impact of various factors, including the treatment of ions in the axial direction, domain size in the radial direction, and ion temperature, on the behavior of ECDI and MTSI in a representative Hall thruster geometry.

## III. Linear Perturbation Theory: ECDI and MTSI

Throughout the rest of the work, the applied, axial electric field will be in the x-direction,  $\mathbf{E} = E_0 \hat{x}$ , the applied, radial magnetic field will be in the z-direction,  $\mathbf{B} = B_0 \hat{z}$ , and the resulting azimuthal  $E \times B$  drift will be in the -y-direction. The electrons drift with a velocity  $\mathbf{U}_d = -E_0/B_0 \hat{y}$  with respect to the unmagnetized ions. In this analysis, only singly-charged ions are considered. Both ECDI and MTSI are facilitated by the coupling of the ion acoustic mode to the electron Bernstein modes when Doppler-shifted into the  $E \times B$  drift frame. The fastest-growing ECDI modes are those that propagate purely in the azimuthal direction. When there is a non-zero component along the magnetic field, i.e., nonzero  $k_z$ , the ECDI resonances thermally broaden due to the motion of the electrons along the magnetic field lines. Therefore, unless there is some physical mechanism that drives a non-zero  $k_z$  component, ECDI will tend to propagate purely in the azimuthal direction during the linear growth stage of the instability. The dispersion relation for ECDI, assuming that the equilibrium velocity distribution function (VDF) is an isotropic Maxwellian, is given by Eq. 1:



$$0 = 1 - \frac{T_e}{2T_i} Z' \left( \frac{\omega - \mathbf{k} \cdot \mathbf{U}_i^+}{\sqrt{2}k v_{\text{th},i}} \right) + \frac{1}{k^2 \lambda_D^2} \left[ 1 + \frac{\omega - \mathbf{k} \cdot \mathbf{U}_d}{\sqrt{2}k_{\parallel} v_{\text{th},e}} e^{-k_{\perp}^2 r_L^2} \sum_{n=-\infty}^{\infty} I_n(k_{\perp}^2 r_L^2) Z \left( \frac{\omega - \mathbf{k} \cdot \mathbf{U}_d + n\omega_{ce}}{\sqrt{2}k_{\parallel} v_{\text{th},e}} \right) \right], (1)$$

where Z is the plasma dispersion function with Z' being its first derivative, and  $I_n$  is the modified Bessel function of the first kind. For long wavelengths along the magnetic field, i.e.,  $k_z \lambda_D \ll 1$ , ECDI is characterized by a resonant structure, with a resonance between every cyclotron harmonic. However, for plasma conditions relevant to Hall thrusters, as the value of  $k_z \lambda_D$  increases to 0.05 and beyond, the ECDI transitions from a resonant to a broadband, ion acoustic-like structure.

On the other hand, MTSI requires a non-zero  $k_z$  component in order to exist. Because MTSI requires a non-zero  $k_z$ , while ECDI does not, these modes are typically distinguished from one another, even though the full ECDI dispersion relation contains the information about the MTSI mode. Mathematically, MTSI can be thought of as the limit of ECDI in which  $|\omega - \mathbf{k} \cdot \mathbf{U}_d| \ll \omega_{ce}$  such that only the n=0 term is retained in the electron susceptibility. The MTSI dispersion relation is given by:

$$0 = 1 - \frac{T_e}{2T_i} Z' \left( \frac{\omega - \mathbf{k} \cdot \mathbf{U}_i^+}{\sqrt{2} k v_{\text{th},i}} \right) + \frac{1}{k^2 \lambda_D^2} \left[ 1 - e^{-k_\perp^2 r_L^2} - \frac{1}{2} e^{-k_\perp^2 r_L^2} I_0(k_\perp^2 r_L^2) Z' \left( \frac{\omega - \mathbf{k} \cdot \mathbf{U}_d}{\sqrt{2} k_\parallel v_{\text{th},e}} \right) \right], \quad (2)$$

where  $Z'(\zeta) = -2[1 + \zeta Z(\zeta)]$  has been used to rewrite the electron susceptibility in terms of Z'. For Hall thruster plasmas, the MTSI resonance occurs around  $k_z\lambda_D = 0.1 - 0.2$ . Furthermore, the wavelength along the magnetic field needs to be long enough such that the instability does not disappear, i.e., ECDI transition from resonant to broadband structure. Typically, this means that  $k_z\lambda_D \leq 0.03$ . While the growth rates of the MTSI mode that are predicted by linear perturbation theory are smaller than those of ECDI, it has been demonstrated by Muschietti and Lembège<sup>20</sup> that the MTSI mode can compete with, and even dominate, ECDI during the nonlinear saturation period of instability development. Previous work has been done by the authors<sup>21</sup> to solve these dispersion relations in the general 3D case. This solutions will serve as benchmarks for the PIC results to follow.

## IV. Code Structure

The 3D PIC code that is used for this analysis was been previously discussed and verified by the authors, <sup>22</sup> so the code structure will only be highlighted here, and instead, emphasis will be placed on subroutines that have been added since that publication.

The 3D PIC software that was developed in C++ uses Message Passing Interface (MPI) to decompose the three-dimensional domain across all processors into subdomains. Each processor stores a local copy of the fluid/field quantities are stored on a local grid and all macroparticle information for those macroparticles currently residing within the processor boundary. Because the phenomena of interest are electrostatic, only Poisson's equation is solved for the electrostatic potential. This is accomplished with HYPRE<sup>23</sup> via generalized minimal residual (GMRES) and the pipe flow multi-grid (PFMG) preconditioner. The particle and field updates use an explicit scheme.

A second-order accurate, central differencing scheme is use to solve Poisson's equation, with the electrostatic potential,  $\phi$ , defined at the cell centers. The components of the electric field,  $E_x$ ,  $E_y$ , and  $E_z$  are each defined on their own staggered grid such that each component lies on the face to which it is normal. This eases the complexity of calculating these electric field components, as only the two adjacent  $\phi$  values are used. Figure 1 shows this discretization scheme. Instead of outputting the electric field components on these staggered grids, they are averaged to the cell centers such that they are collocated with the electrostatic potentials.

To study the impact of a forced signal in the radial direction on the development of MTSI, a capability had to be implemented that allowed for non-uniform macroparticle initialization. To accomplish this, macroparticles are still placed uniformly within each cell. However, the number of macroparticles within each cell is calculated by using a local density of  $n_0[1 - A\sin(2\pi z/L_z)]$ , with the amplitude A being 0.2 such that the density varies between 80% and 120% of the prescribed quasineutral particle density. Both the electrons and ions are perturbed in this way to maintain quasineutrality initially throughout the domain.



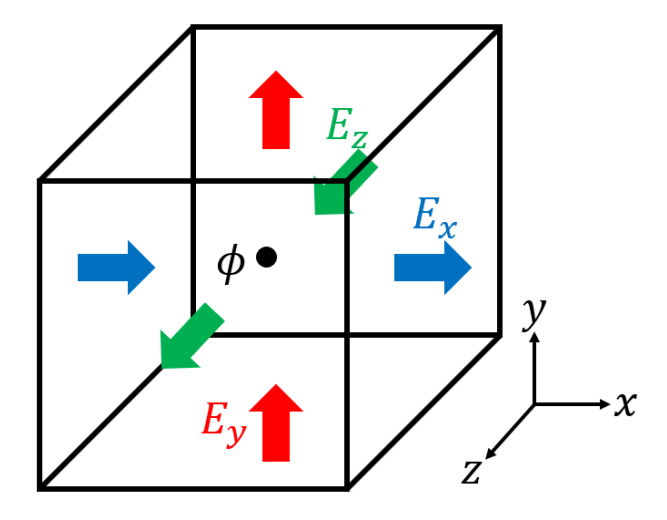


Figure 1. Schematic for the structure of  $\phi$ ,  $E_x$  (blue),  $E_y$  (red), and  $E_z$  (green), illustrated on a 3D grid cell.

# V. Results

# A. Model Description

To isolate the geometrical effects from the effects exclusively due to the 3D nature of ECDI and MTSI, a three-dimensional box geometry is chosen for the following analysis. Two boundary conditions will be considered for the radial direction: periodic and grounded Dirichlet walls. In the case with Dirichlet walls, electrons that hit the wall are deleted. However, when an ion hits the wall, an ion/electron pair is reinjected in the domain proportional to the electron density, simulating a "fake" ionization source. This means that the number of ion macroparticles within the simulation domain remains constant, while the number of electron macroparticles will adjust itself to balance the ionization source with the electron wall flux. The ion/electron pairs are reinjected using an isotropic Maxwellian VDF with temperatures given by  $T_{i,0}$  and  $T_{e,0}$  in Table 1, respectively. The simulation parameters for the baseline case are given in Table 1. Using 256 processors, the case given in Table 1 is able to complete about one microsecond of simulation time per day of wall time. The time step was chosen to satisfy the inequality  $\omega_{pe}\Delta t < 0.2$ . In this case, based on the initial plasma density,  $\omega_{pe}\Delta t = 0.063$ . Both the ion and electron species are initialized with Maxwellian VDFs with zero bulk velocities.

## B. Effect of Continuous Acceleration of Ions

Because the axial direction uses periodic boundary conditions, without special consideration given to the unmagnetized ions, they will continuously accelerate under the influence of the applied axial electric field. As a result, their kinetic energy will grow unbounded, leading to unphysical axial ion bulk velocities. Therefore, to counteract the periodic, axial boundary condition, the ions are only accelerated by forces due to the perturbed electric field, i.e.,  $E' = E - E_0$ , where  $E_0$  is the applied electric field in Table 1. This way, the ions still respond self-consistently with the plasma waves generated by any instabilities present, but they do not continuously accelerated from  $E_0$ . In Hall thrusters, the ion axial bulk velocity in the plume is relatively constant<sup>14</sup> because the axial electric field is much smaller than near the exit of the discharge chamber.

The investigation into the effect of this treatment of the ions was undertaken using helium to speed up the computation. In the case in which the ions do feel the applied, DC electric field, the helium ions acquire an axial ion bulk velocity of 800,000 m/s during the 4  $\mu$ s simulation. Comparing this value with previous 2D PIC simulations,<sup>14</sup> which considered xenon ions, this axial bulk velocity is about 55 times larger. However, because the mass ratio of xenon and helium ions is 65.5, the axial ion bulk velocity are in the continuously accelerated case is still realistic to what would be expected during the steady state operation of an  $E \times B$  plasma with parameters given by Table 1. Increasing the simulation runtime beyond 5-10  $\mu$ s would lead to unphysically large axial ion bulk velocities, so this technique is still reasonable for the 4  $\mu$ s. In the case in which the ions do not feel the applied, DC electric field, the helium ions do not acquire a mean axial bulk



Table 1. Table of simulation and plasma parameters for the 3D cross-field instability test case.

Plasma Parameter	Value
Applied Electric Field	$7520~\hat{x}~\mathrm{V/m}$
Applied Magnetic Field	$0.015~\hat{z}~\mathrm{T}$
Density	$5 \times 10^{16} \ m^{-3}$
$T_{e,0}$	25 eV
$T_{i,0}$	$0.25~{ m eV}$
Ion Species	Helium/Argon
Simulation Parameters	Value
Domain Length $(L_x = L_y = L_z)$	0.02 m
Number of Cells $(N_x = N_y = N_z)$	128
Time Step	5 ps
Simulation Time	$4~\mu \mathrm{s}$
Particles per Cell per Species	100

velocity. From the perspective of studying ECDI and MTSI, this is perfectly adequate, as this is equivalent to Doppler-shifting into the ion rest frame. Therefore, for the rest of the analysis, the ions will evolve only under the influence of the perturbative electric field.

#### C. Effect of Radial Boundary Condition

The radial boundary conditions have a large impact on the appearance of the MTSI mode. While the ECDI mode appears regardless of the field boundary condition in the radial direction, the same cannot be said for the MTSI mode. Because the MTSI mode requires a nonzero component of the wavevector along the magnetic field, there must be a mechanism for the plasma to sustain dynamics in this direction. In an  $E \times B$  device, the relative azimuthal  $E \times B$  drift of the electrons with respect to ions serves as the mechanism that sustains the ECDI and MTSI dynamics in the azimuthal direction. Previous work <sup>16</sup> has demonstrated that plasma-wall interactions, like the diffusion of ions toward the radial walls, are a key mechanism for initiating the MTSI. If the radial direction is treated as periodic, then there is no sheath-driven diffusion of the ions. Furthermore, there is no length-scale that is selected by the physical system that creates the long-wavelength component of MTSI along the magnetic field lines.

Because the ratio of  $T_e/T_i$  is initially equal to 100, to a very good approximation, it can be accurately assumed that the ions are cold.<sup>19</sup> Denig and Hara<sup>19</sup> have previously demonstrated that the largest ECDI growth rates occur for  $k_x = k_z = 0$ . The behavior of the growth rate of ECDI and MTSI as a function of the normalized azimuthal wavenumber  $k_y \lambda_D$  for the case in Table 1 is given in Fig. 2. Similarly, because the domain size is 2 cm in each direction, and the smallest possible, nonzero, radial wavenumber is  $k_z \lambda_D = 0.0522$ , the growth rate of ECDI and MTSI are also given in Fig. 2 for  $k_z \lambda_D = 0.0522$ .

Because ECDI behaves resonantly for  $k_z\lambda\ll 1$ , the dominant ECDI mode occurs at  $k_y\lambda_D=0.94$  with a growth rate of  $0.44\omega_{pi}$ . In the simulation, due to the finite size of the box, the MTSI mode occurs at  $k_y\lambda_D=0.21$  and  $k_z\lambda_D=0.0522$  with a growth rate of  $0.05\omega_{pi}$ . The cold ion assumption is valid during the first microsecond of simulation time, when the ion temperature has not increased too much from its initial value. This is also the time during which the linear growth stages of ECDI and MTSI occur, which is the limit of predictability for the linear perturbation theory discussed in Sec. III, so the cold ion assumption should reliably predict the behavior of the instabilities.



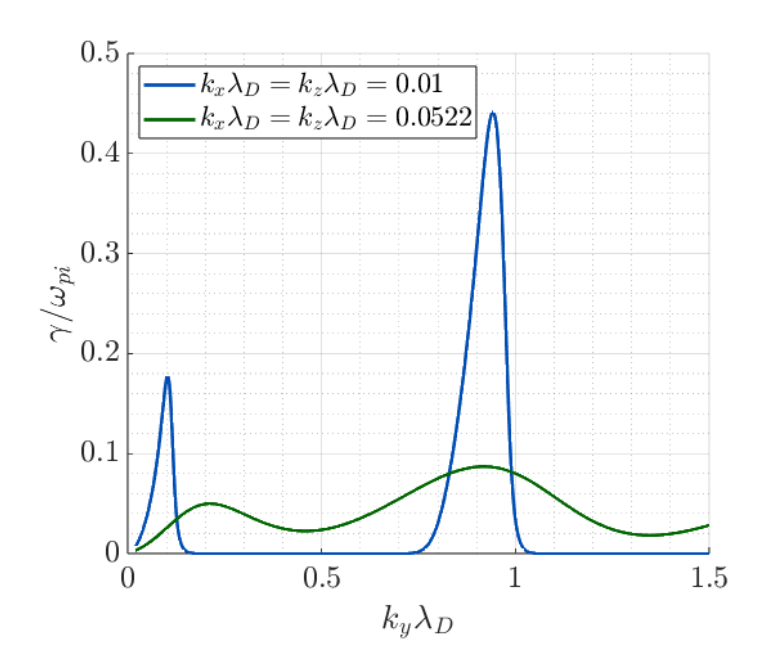


Figure 2. Growth rate,  $\gamma/\omega_{pi}$ , from the dispersion relation for ECDI, i.e., Eq. 1, with plasma parameters from Table 1, and  $k_x\lambda_D=k_z\lambda_D=0.01$  (blue) and  $k_x\lambda_D=k_z\lambda_D=0.0522$  (green) as a function of  $k_y\lambda_D$ . Note that  $k_x\lambda_D=k_z\lambda_D=0.01$  are used instead of 0 because the root finder uses the plasma dispersion function, not the dominant term in the asymptotic limit, so setting  $k_z$  exactly to 0 in the denominator results in undefined behavior.

#### 1. Periodic Radial Boundary Condition

Here, in the case of the periodic radial boundary condition, in an attempt to force an MTSI mode, the initial ion and electron density profiles are perturbed by a sine wave with a wavelength equal to half of the radial domain size. With an initial electron temperature of 25 eV, this wavelength corresponds to a normalized wavenumber along the magnetic field of 0.1044. The amplitude of this perturbation is equal to 20% of the initial density value. The longest wavelength that can be sustained along the magnetic field in this 2 cm square domain corresponds to a  $k_z \lambda_D$  value of 0.0522. This mode has a higher growth rate than the mode that was forced initially by the density perturbation, so in long times, this mode would be expected to dominate.

The growth rates of different modes within the system can be found through performing a 3D FFT on the azimuthal electric field data from the 3D PIC simulation. The 3D array of Fourier amplitudes in wavenumber space, i.e.,  $\hat{E}_y \hat{E}_y^*(k_x, k_y, k_z)$ , are then taken at the specific wavenumbers predicted by kinetic theory to contain the ECDI and MTSI modes. The results are given in Fig. 3. The ECDI mode begins growing almost immediately at a growth rate that agrees very well with the analytical growth rate from linear perturbation theory, before saturating around 0.5  $\mu$ s. Meanwhile, the MTSI mode never grows, despite an initial density perturbation in the z-direction being forced. Because the radial boundary condition is periodic, the ions and electrons are able to move along the magnetic field lines and short out the initial density perturbation such that by the time MTSI would start to grow, there is no longer a nonzero  $k_z$ , a necessary condition for the appearance of MTSI.

#### 2. Radial Wall Boundary Condition

With grounded, radial walls, the behavior of the system is quite different. The  $k_z\lambda_D - 0.1022$  density perturbation is still used initially for the sake of comparison with the periodic case, but other simulations, not shown here, demonstrate that this initial density perturbation is not necessary to initiate MTSI when there are radial walls present. The diffusion of the unmagnetized ions to the wall, forming a sheath, along with the wall separation being a physical length scale for the wave, ensure that the MTSI mode appears with a radial wavenumber equal to one domain-size wavelength. The same Fourier amplitude data is plotted



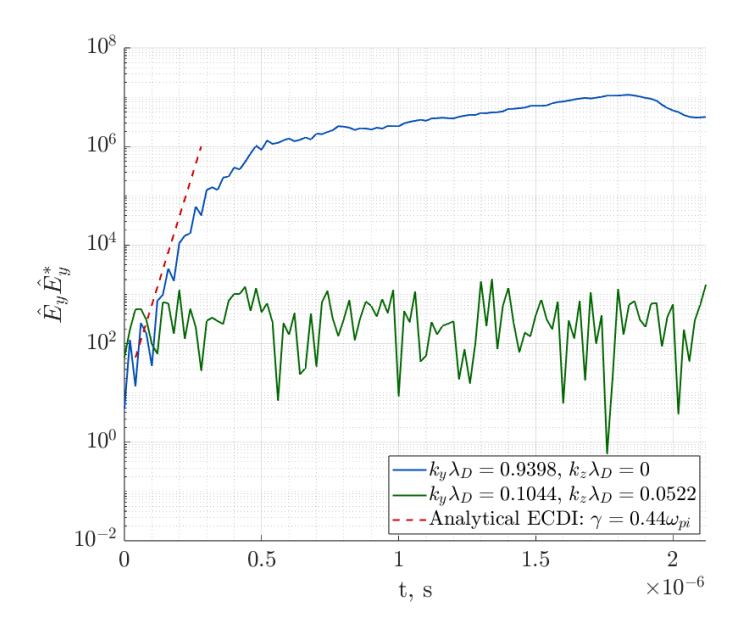


Figure 3. The Fourier amplitudes of the ECDI mode (blue) and the MTSI mode (green) as functions of time. The analytical growth rate for the ECDI mode is given by the red line.

in Fig. 4 for the case of the grounded radial wall.

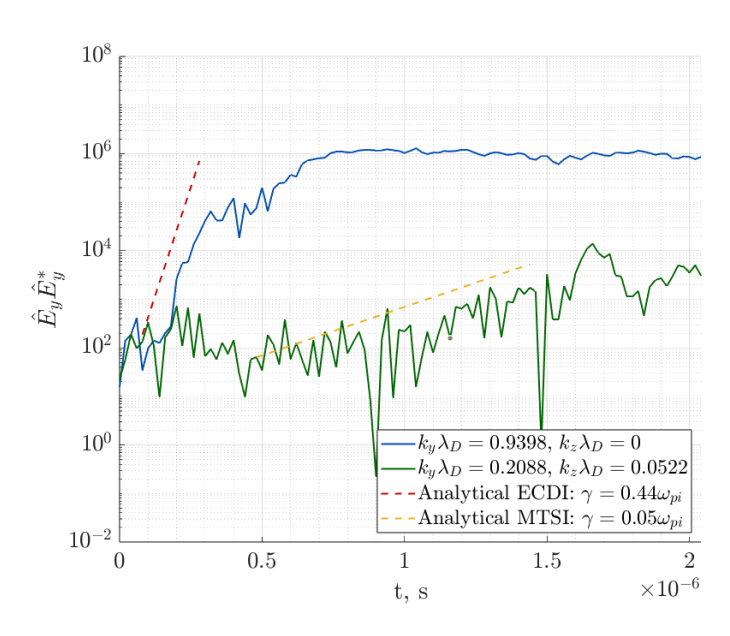


Figure 4. The Fourier amplitudes of the ECDI mode (blue) and the MTSI mode (green) as functions of time. The analytical growth rate, computed by Eq. 1, for the ECDI mode is given by the red line, and the analytical growth rate, computed by Eq. 2, for the MTSI mode is given by the yellow line.

In Fig. 4, the ECDI grows at the same rate as in Fig. 3, indicating that the dominant ECDI mode does not have a component of its propagation along the magnetic field line, which agrees with the kinetic theory. <sup>19</sup> Conversely, the MTSI mode is now seen to be slowly growing with time, as expected for an MTSI mode with a radial wavenumber of  $k_z\lambda_D=0.0522$ . The analytical growth rate of  $0.05\omega_{pi}$  agrees very well with the simulation results. The MTSI signal is much noisier than the ECDI signal because the amplitude of the MTSI mode is roughly three orders of magnitude smaller than the ECDI mode this early in the simulation. Should the simulation be run for a longer time, the MTSI mode would saturate at a similar amplitude to the



ECDI mode. Therefore, the MTSI mode is very sensitive to the boundary conditions employed in the radial direction, as dynamics along the magnetic field are essential for the MTSI mode's existence. This supports previous findings from 2D radial-azimuthal simulations. Which suggest that the plasma-wall interaction is crucial to the formation of MTSI.

## D. Effect of Ion Temperature

The authors have previously performed theoretical analysis on the impact of finite ion temperature on the nature of ECDI and MTSI.<sup>19</sup> From these studies, ion Landau damping decreases the growth rate of ECDI more strongly than the growth rate of MTSI because ECDI is a short-wavelength instability. Short-wavelength, i.e., large wavenumber, modes are more strongly affected by Landau damping. For  $k_z \lambda_D = 0.01$  and  $T_e = 25$  eV, ECDI was found to be completely damped by ion Landau damping for  $T_i/T_e = 0.544$ . Meanwhile, because MTSI is a long-wavelength mode, it is not strongly impacted by the warm ion population. In fact, in order for MTSI to be damped via ion Landau damping at these plasma conditions, the ion population would need to be warmer than the electron population, which is not the case in Hall thrusters.

To demonstrate the ion Landau damping effect on MTSI, four different cases were run:  $T_{i,0} = 0.25$  eV,  $T_{i,0} = 1$  eV,  $T_{i,0} = 2$  eV, and  $T_{i,0} = 5$  eV. The rest of the plasma parameters are given in Table 1, and the radial boundary condition considered here uses radial walls. The growth rates from each simulation, calculated with an exponential fit during the linear growth stage of the instability, are shown for ECDI and MTSI, and compared with theory in Fig. 5.

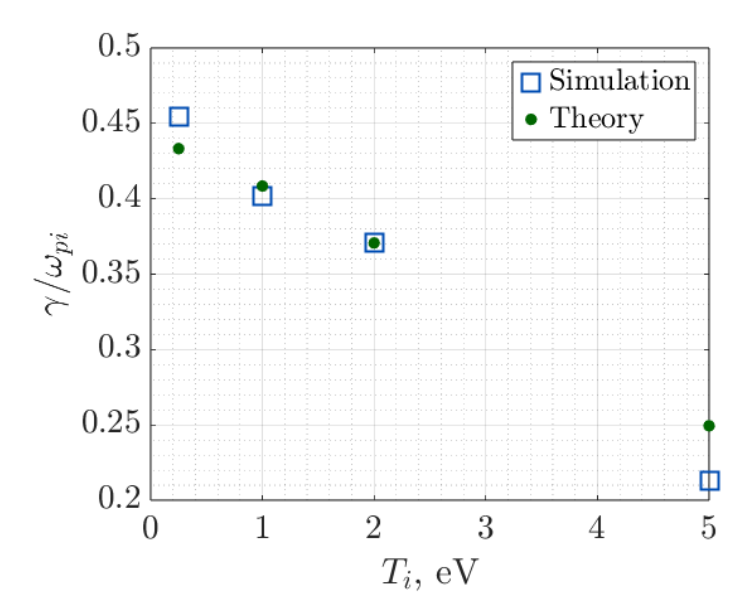


Figure 5. The normalized growth rate versus the ion temperature from both 3D PIC simulations (blue) and linear perturbation theory calculations (green). The points for  $T_i = 2$  eV case are on top of one another.

There is a very good agreement between the 3D PIC simulations and the linear perturbation theory. For each ion temperature that was simulated, the value of the growth rate from the PIC code was within 10% of the theoretical growth rate using Eq. 1. Like in Figs. 3-4, the Fourier amplitudes are a bit noisy, which could be improved by increasing the number of particles per cell from 100, but for the sake of computational cost, these more expensive cases are not presented here. Because of this noise and because the MTSI growth rate is much smaller than the ECDI growth rate, the MTSI mode can be drowned out by noise for the higher ion temperature cases. There is a consistent trend that the electrostatic energy in the ECDI and MTSI modes decreases as ion temperature increases. This effect cannot be predicted by linear perturbation theory, as this is a nonlinear phenomenon that impacts the saturation of these instabilities. In fact, for the  $T_{i,0} = 5$  eV case, the short-wavelength ECDI mode is not visually apparent unless one looks at the Fourier transformed data. A comparison between the azimuthal electric field is illustrated for two cases in Fig. 6:  $T_{i,0} = 1$  eV and  $T_{i,0} = 5$  eV.

For  $T_{i,0} = 1$  eV, the maximum azimuthal electric field value is about 11,700 V/m, while the maximum



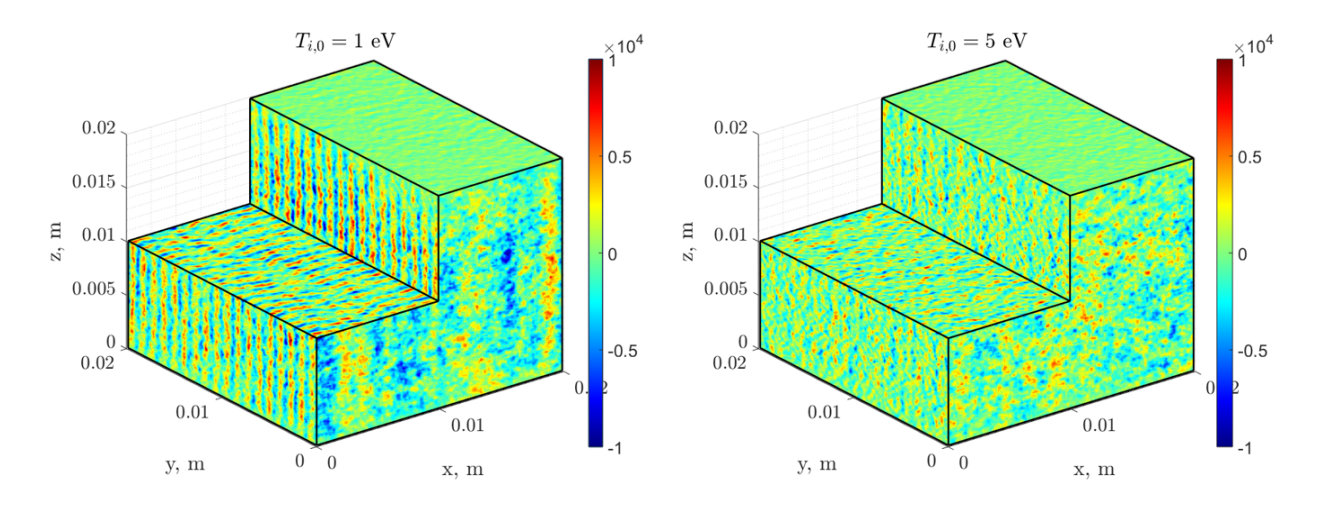


Figure 6. The left image shows the azimuthal electric field for  $T_{i,0} = 1$  eV, and the right image shows the azimuthal electric field for  $T_{i,0} = 5$  eV. Both snapshots are shown at  $0.6~\mu s$  with the colorbar from  $10^4$  to  $10^4$  V/m.

azimuthal electric field value in the  $T_{i,0}=5$  eV case is only 10,000 V/m. This is consistent with the lower growth rate of ECDI for warmer ions. Furthermore, for the plasma parameters in Table 1, there should be 18 wavelengths of ECDI in the domain. This is true, regardless of ion temperature. However, the amplitude of the perturbative  $E_y$  is much lower in the  $T_{i,0}=5$  eV case, so that structure is much less apparent in the right half of Fig. 6. Finally, for the colder ions cases, once ECDI saturates, the electrostatic energy remains roughly constant in time. However, for the  $T_{i,0}=2$  eV and  $T_{i,0}=5$  eV cases, the ion Landau damping persists even after the instability saturates, resulting in the total electrostatic energy contained within the ECDI modes decreasing until the plasma becomes quiescent once more.

### VI. Conclusion

The development of an explicit, electrostatic 3D PIC code has facilitated the verification of the 3D linear perturbation theory of ECDI and MTSI, including warm ion effects. This verification includes the correct prediction of ECDI growth rates as a function of ion temperature and the correct wavenumber. Furthermore, the radial boundary condition was found to be crucial to the appearance of MTSI within the cross field configuration. With a periodic boundary condition, the instability never appears, but with grounded, radial walls such that a plasma sheath forms, the MTSI mode exists. The diffusion of ions toward the walls, forming a plasma sheath, is hypothesized to reinforce the  $k_z$  component of the ECDI/MTSI system. Because the MTSI mode has been demonstrated to be as important as ECDI in terms of its saturation amplitude, <sup>20</sup> understanding the role of the plasma-wall interaction is important for the potential mitigation of this instability in Hall thruster designs. These 3D PIC simulations, while computationally expensive, give more insight into the nature of the kinetic instabilities in Hall thrusters.

# VII. Acknowledgments

This work was supported by a NASA Space Technology Graduate Research Opportunity, under Grant No. 80NSSC21K1273, and NASA through the Joint Advanced Propulsion Institute, a NASA Space Technology Research Institute under Grant No. 80NSSC21K1118. Finally, we would like to acknowledge Stanford University's HPCs for computational resources.

# References

<sup>1</sup>Kaganovich I D, Smolyakov A, Raitses Y, Ahedo E, Mikellides I G, Jorns B, Taccogna F, Gueroult R, Tsikata S, Bourdon A, Boeuf J P, Keidar M, Powis A T, Merino M, Cappelli M, Hara K, Carlsson J A, Fisch N J, Chabert P, Schweigert I, Lafleur T, Matyash K, Khrabrov A V, Boswell R W and Fruchtman A 2020 Physics of Plasmas 27 120601



- $^2$ Tsikata S 2009 Small-scale electron density fluctuations in the Hall thruster investigated by collective light scattering Ph.D. thesis Ecole Polytechnique
  - <sup>3</sup>Tsikata S, Honoré C and Grésillon D 2013 Journal of Instrumentation 8 C10012
  - <sup>4</sup>Tsikata S and Minea T 2015 Physical Review Letters 114(18) 185001
  - <sup>5</sup>Forslund D W, Morse R L and Nielson C W 1970 Physical Review Letters 25(18) 1266–1270
  - <sup>6</sup>Forslund D W, Morse R L and Nielson C W 1971 Physical Review Letters 27(21) 1424–1428
  - $^7\mathrm{Gary}$ S P and Sanderson J J 1970 Journal of Plasma Physics 4 739–751
  - $^8\mathrm{McBride}$  J B, Ott E, Boris J P and Orens J H 1972 The Physics of Fluids 15 2367–2383
  - $^9 {\rm Lashmore\text{-}Davies}$  C and Martin T 1973  $Nuclear\ Fusion\ {\bf 13}\ 193{-203}$
  - $^{10} \mathrm{Lafleur}$  T, Baalrud S D and Chabert P 2016 Physics of Plasmas  $\mathbf{23}$  053503
- $^{11} \mathrm{Smolyakov}$ A, Zintel T, Couedel L, Sydorenko D, Umnov A, Sorokina E and Marusov N2020 Plasma Physics Reports 46 496-505 ISSN 1562-6938
  - <sup>12</sup>Janhunen S, Smolyakov A, Sydorenko D, Jimenez M, Kaganovich I and Raitses Y 2018 Physics of Plasmas 25 082308
- <sup>13</sup>Charoy T, Boeuf J P, Bourdon A, Carlsson J A, Chabert P, Cuenot B, Eremin D, Garrigues L, Hara K, Kaganovich I D, Powis A T, Smolyakov A, Sydorenko D, Tavant A, Vermorel O and Villafana W 2019 *Plasma Sources Science and Technology* 28 105010
  - $^{14}{\rm Hara~K}$ and Tsikata S 2020 Physical Review E  ${\bf 102}(2)$ 023202
  - <sup>15</sup>Petronio F, Tavant A, Charoy T, Alvarez Laguna A, Bourdon A and Chabert P 2021 Physics of Plasmas 28 043504
- <sup>16</sup>Villafana W, Petronio F, Denig A C, Jimenez M J, Eremin D, Garrigues L, Taccogna F, Alvarez-Laguna A, Boeuf J P, Bourdon A, Chabert P, Charoy T, Cuenot B, Hara K, Pechereau F, Smolyakov A, Sydorenko D, Tavant A and Vermorel O 2021 Plasma Sources Science and Technology 30 075002
  - <sup>17</sup>Taccogna F and Minelli P 2018 Physics of Plasmas 25 061208 ISSN 1070-664X
  - <sup>18</sup>Villafana W, Cuenot B and Vermorel O 2023 Physics of Plasmas **30** 033503
  - <sup>19</sup>Denig A C and Hara K 2025 Physics of Plasmas 32 022110 ISSN 1070-664X
  - <sup>20</sup>Muschietti L and Lembège B 2013 Journal of Geophysical Research: Space Physics 118 2267–2285
  - <sup>21</sup>Denig A C and Hara K 2023 Physics of Plasmas **30** 032108
  - $^{22}\mathrm{ADenig}$  and Hara K 2024  $\mathit{IEPC}\text{-}2024\text{-}852$
- $^{23}$  Falgout R D and Yang U M 2002 hypre: A library of high performance preconditioners Computational Science ICCS 2002 ed Sloot P M A, Hoekstra A G, Tan C J K and Dongarra J J (Berlin, Heidelberg: Springer Berlin Heidelberg) pp 632–641 ISBN 978-3-540-47789-1

